Failure analysis of adhesively-bonded skin-to-stiffener joints: metal-metal vs. composite-metal

Sofia Teixeira de Freitas[a,*], Jos Sinke[a]

[a] *Delft University of Technology, Kluyverweg 1, 2629 HS Delft, The Netherlands*

Abstract

The purpose of this research is to evaluate the performance of two adhesively bonded skin-to-stiffener connections: composite stiffener bonded to a Fiber Metal Laminate (FML) skin, representing a hybrid joint, and an Aluminium stiffener bonded to a FML skin, representative for a metal joint. The bonded joints were tested using stiffener pull-off tests (SPOT), which is a typical set-up used to simulate the structural behaviour of full-scale components subject to out-of-plane loading, such as internal pressure of a fuselage or leading edge low pressure zone. In the hybrid joint, the damage initiates at the central noodle of the composite stiffener. Unstable delamination then propagates from the noodle to the tip of the stiffener foot, preferably through the stiffener foot plies (> 90% of inter/ intra-laminar failure) and, in limited areas, through the adhesive bond line (< 10% of cohesive failure). In the metal joint, the failure starts at the tip of the stiffener foot at the adhesive bond line. Unstable debonding then propagates along the stiffeners foot. The complete failure occurs in the adhesive bond line (100% cohesive failure). The loads associated with > 90% of inter/intra laminar failure of the composite stiffener (hybrid joint) are 40% to 60% lower than the ones associated with 100% cohesive failure (metal joint). This research identifies that in order to use the full capacity of adhesively bonded hybrid joints, the adhesion between carbon fibres of the composite laminate, ie intralaminar strength, must be improved. Otherwise, Aluminium stringers are still very competitive.

Keywords:

Adhesive bonding, skin-to-stiffener connection, composite-to-aluminium joints

*Corresponding author. Tel: +31 15 28 82287 Fax: +31 15 278 1151

Email addresses: `S.TeixeiraDeFreitas@tudelft.nl` (Sofia Teixeira de Freitas), `J.Sinke@tudelft.nl` (Jos Sinke)

1. Introduction

Due to their superior specific strength and stiffness when compared to the traditional metals, composite laminates are becoming the first choice in aircraft applications. A true testimony of this fact is the newest civil aircraft Boeing 787 applying materials of which are 50% composites and 50% metals. With such hybrid structures, composite parts often need to be joined with metal parts. Adhesive bonding offers major advantages for joining different materials when compared to traditional mechanical riveting. Moreover, adhesively bonded joints are the most suitable technology for joining composite materials, since it avoids drilling, stress concentrations and fiber-cutting which can significantly decrease the performance of the composite laminate. Therefore, the application of adhesive bonded joints has been developed in parallel with composites [1].

Most of the research in composite-to-metal bonded joints is limited to coupon tests. Single- and double-lap joints (SLJ and DLJ) have been used to evaluate the shear strength of bonded composite-to-aluminium joints [2–4]. Double cantilever beam (DCB) hybrid specimens are used to characterize the crack propagation behavior and giving input data for fracture mechanics [5, 6]. Since adhesion is one of the key components for guarantying the integrity of bonded joints, new peel tests have been developed in order to assess the adhesion quality of composite-to-metal bonded joints [7].

However in order to succeed, composite-to-metal bonded joints also need to prove their performance in structural applications and not only at the coupon level. In aircraft applications, skin-to-stiffener joints are very common in fuselage panels and wings. Due to the impossibility to test different design concepts and materials at a full-scale, sub-components test simulate the loading and boundary conditions of the full-scale components. Stiffener Pull-Off Tests (SPOT) is one of the sub component tests that simulates out-of-plane loading in skin-to-stiffener joints, such as internal pressure of the fuselage skin and low pressure zone of leading edges [8–10].

Stiffener Pull-Off Tests have been extensively used to evaluate the performance of different design concepts and structural features in skin-to-stiffener joints. The aim of these new features is to try to identify the ones that offer more load capacity or higher toughness [10–12]. SPOT are also used to identify the failure sequence and failure modes in order to help designers to predict the behaviour of these complex joints [13]. However, most of the research is performed in either co-cured composite-skin to composite-stiffener or bonded metal-skin to metal-stiffener [13, 14]. Few research is available in skin-to-stiffener hybrid joints.

With the increasing use of composites over metals, attention should be paid on how this material replacement influences the structure's behaviour. In this research, the aim is to compare the performance of two adhesively bonded skin-to-stiffener joints; metal skin to metal stiffener and metal skin to composite stiffener (hybrid). Stiffener-pull-off tests (SPOT) were conducted in order to characterize the failure mechanism and the load carrying capacity of both types of joint. The conventional metal solution is compared with the new solution for hybrid structures.

2. Materials and Specimens

Stiffener pull-off test specimens were manufactured by bonding the stiffener to the skin. For the metal joint an Aluminium stiffener was bonded to a Fiber Metal Laminate (FML) skin. For the composite-to-metal hybrid joint, a Carbon Fibre Reinforced Polymer (CFRP) stiffener was bonded to a FML skin.

2.1. Materials

The Fiber Metal Laminate (FML) skin was Glare 5-3/2-0.3, which consists of three 2024-T3 aluminium alloy layers 0.3 mm thick, bonded together with glass prepregs S2-glass/FM-94 with the layup $[0^\circ/90^\circ/90^\circ/0^\circ]$. The skin layup is therefore $[Al/[0^\circ/90^\circ/90^\circ/0^\circ]/Al/[0^\circ/90^\circ/90^\circ/0^\circ]/Al]$. The outer faces of the skin are Aluminium layers (metal). The skin was cured in the autoclave according to the standard procedure for Glare (4 bars, 60 min at 120 °C). The aluminium surfaces were pre-treated with chromic acid anodizing and primed with BR 127 (Cytec Engineered Materials, Tempe, Arizona, USA).

The Aluminium stiffener was an extruded inverted T-shape stiffener of 2024-T3 aluminium allow. The surface pre-treatment was identical to the FML skin aluminium surfaces.

The CFRP stiffeners were prepared from unidirectional pre-preg consisting of HexPly 8552 epoxy matrix in combination with AS4 carbon fiber (Hexcel Corporation, Stamford, Connecticut, USA). The CFRP stiffener was an inverted T-shape stiffener. It was manufactured from two laminates, each with layup $[+45^\circ/0^\circ/-45^\circ/90^\circ/+45^\circ]_S$, which were put back to back in a L-shape. The noodle region was filled with 0° fibers. The stiffener was cured at 180 °C for 120 min in the autoclave. Prior to bonding, the CFRP-stiffener-foot surfaces were abraded with sand paper and then wiped clean with an acetone-soaked cloth. Figure 1 shows the configuration of both stiffeners.

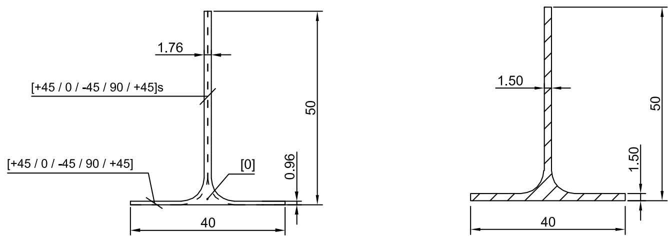

(a) CFRP stiffener (b) Aluminium stiffener

Figure 1: Stiffeners' configuration (dimension in mm).

Two adhesives were used on both configurations; AF 163-2K.06 (3M, Minnesota, USA) and EA9696.060 PSF K (Henkel, Düsseldorf, Germany). Both are epoxy film adhesives with a curing temperature of 120 °C for 90 min in the autoclave. The adhesives were chosen after performing screening tests on ten adhesives [15]. These two adhesives scored the best results in terms of good adhesion to metals and to composites, and in terms of apparent average shear strength (higher than 20 MPa). AF 163-2 has been on the market for many years and it is being used for metal bonding and, more recently, for composite bonding. EA 9696 is especially tailored for high toughness applications. This last feature can be of major importance for the hybrid joint, since we are joining materials with different coefficient of thermal expansion.

Tables 1 and 2 show the mechanical properties taken from literature and from the Technical Data Sheet (TDS) of the materials used.

Table 1: Mechanical properties of the isotropic materials used.

	E_t (MPa)	σ_{yt} (MPa)	σ_{maxt} (MPa)	ν (-)
Al 2024-T3 [16]	72400	347	420	0.33
AF 163-2 (TDS)	1110	–	48.3	0.34
EA 9696 (TDS)	2082	–	45.9	0.34

2.2. Specimens

The base line of the Pull-off specimens is a Glare skin adhesively bonded with either a CFRP stiffener (hybrid joint) or an Aluminium stiffener (metal joint) at mid span. Both metal and hybrid

Table 2: Mechanical properties of the orthotropic materials used.

	E_1 (MPa)	E_2 (MPa)	ν_{12} (-)	ν_{21} (-)
S2-glass/FM-94 [16]	48900	5500	0.33	0.0371
HexPly-8552/AS4 (TDS)	131000	9240	0.302	0.029

joints were tested using AF 163-2 and EA9696. All specimens were 100 mm wide and the length varied from 200 mm up to 400 mm. Table 3 shows the nomenclature used to reference the four types of specimens.

Table 3: Specimens' nomenclature.

Nomenclature	Skin	Stiffener	Adhesive	Figure
Mt–AF	Glare	Aluminium	AF 163-2	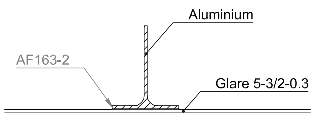
Mt–EA	Glare	Aluminium	EA 9696	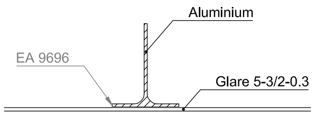
Hy–AF	Glare	CFRP	AF 163-2	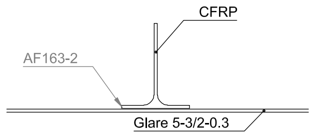
Hy–EA	Glare	CFRP	EA 9696	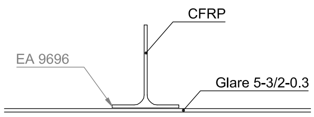

3. Experimental Procedure

3.1. Adhesive material testing

Tensile tests were performed on the bulk adhesive material of AF 163-2U and EA 9696.06 U, in accordance with ISO 527 [17]. The specimens were prepared by a layup of film adhesive without carrier. Bone shape specimens were cut out from the cured adhesive plate. The tests were carried out at displacement control using a testing machine with a load cell of 10 kN. The testing speed was 5 mm/min. A mechanical extensometer was used to measure the specimens elongation during testing.

3.2. *Stringer Pull-Off Tests*

The pull-off test setup is shown in Figure 2. The clamping of the skin was guaranteed by two steel plates on each support, connected to the skin by bolts. A tensile load was applied vertically to the stiffener web (P – see Fig. 2) using a clamp. Pull-off test were performed at different spans; 100 mm , 200 mm and 300 mm (L – see Fig. 2(b)). The tests were conducted in a Dyna Mess servo-pneumatic testing machine (Aachen, Germany), with a 20 kN load cell, at a testing speed of 3 mm/min. The loads and piston displacement were recorded during testing. The tests were performed until there was complete detachment of the stiffener from the skin. Typically, three specimens were tested at the same test conditions. Photographs were taken during testing at regular time intervals and whenever significant changes occurred. After testing, the specimens were dissected and a visual inspection was carried out using optical microscopy to determine the failure modes.

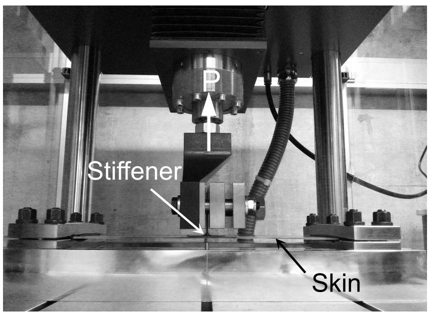

(a)

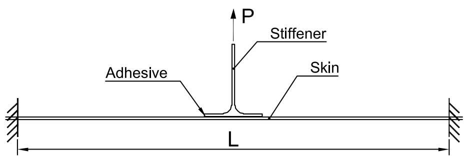

(b)

Figure 2: Pull-off test setup (L=100,200,300 mm).

4. Results

4.1. *Adhesive material behaviour*

Table 4 gives the average values for the Young's modulus E_t, tensile strength σ_{tmax} and failure strain ϵ_{tmax} obtained from the tensile testing performed on the adhesives AF 163-2 and EA 9696.

The adhesives have very similar mechanical properties. The main difference is on the ductility, EA 96969 is more ductile (higher failure strain) than AF 163. However, it was expected that the Young's modulus would also be considerably different between the two adhesives, in accordance with the TDS (see Table 1). The Young's modulus of AF 163-2 is significantly higher than expected which reduces the differences between the two adhesives, and can compromise the intended analysis of the adhesive material effect.

Table 4: Tensile mechanical properties of the adhesive materials (average and coefficient of variation).

Adhesive	E_t(MPa)	Cv (%)	σ_{tmax} (MPa)	Cv (%)	ϵ_{tmax} (%)	Cv (%)
AF 163-2	2155	4%	45.7	3%	5.4	27%
EA 9696	2124	3%	47.8	2%	11.5	14%

4.2. Stringer Pull-Off Tests

Typical load-displacement curves for specimens from different tests series are shown in Figure 3 and Figure 4, for the hybrid joints and metal joints, respectively. Photographs taken during testing showing the damage initiation and crack growth are exemplified for one specimen.

In the hybrid joints, the damage typically initiated at the noodle region of the CFRP stiffener, as shown in Figure 3(b) photograph 2 for the example Hy-AF-100. This damage initiation was accompanied by a sudden drop in the load, as shown in Fig. 3(a) point 2. After that, the specimen continues to carry load, while the crack propagates through the first plies of the stiffener foot and through the web plies at the interface of the two L-shape laminates (see photograph and point 3 in Fig. 3). The maximum load occurs when the stiffener completely detaches from the skin (see photograph and point 4 in Fig. 3). This damage sequence occurred in more than 70% of the hybrid specimens. In the remaining 30%, the damage initiation and final failure were coincident, as for the examples Hy-EA-100 and Hy-AF-300 shown in Figure 3(a). Within the same span, specimens using AF 163-2 or EA 9696 exhibited similar stiffness. As expected, the stiffness is more dependent on the span of the skin than on the adhesive AF 163 or EA 9696.

In the metal joint, the damage sequence is significantly different. The damage initiates at the tip of the stiffener foot through the adhesive layer, as shown in Figure 3(b), photograph 2 for the example Mt-EA-100. The maximum load occurs at this damage initiation – point 2 in Figure 3(a). After that, the load decreases and the crack propagates through the adhesive layer – photograph/point 3 in Fig. 3, until it reaches the opposite side of the stiffener foot and, finally, the stiffener completely detaches from the skin – photograph/point 4 in Fig. 3. For 100 mm span, the damage propagation is more stable than for 200 mm and 300 mm. Typically, for the latter cases the damage initiation occurs simultaneously with final failure. Considering the influence of the skin span and adhesive type, the observation are similar to the hybrid joints; the stiffness is dependent on the skin span but not significantly affected by the adhesive AF 163 or EA 9696.

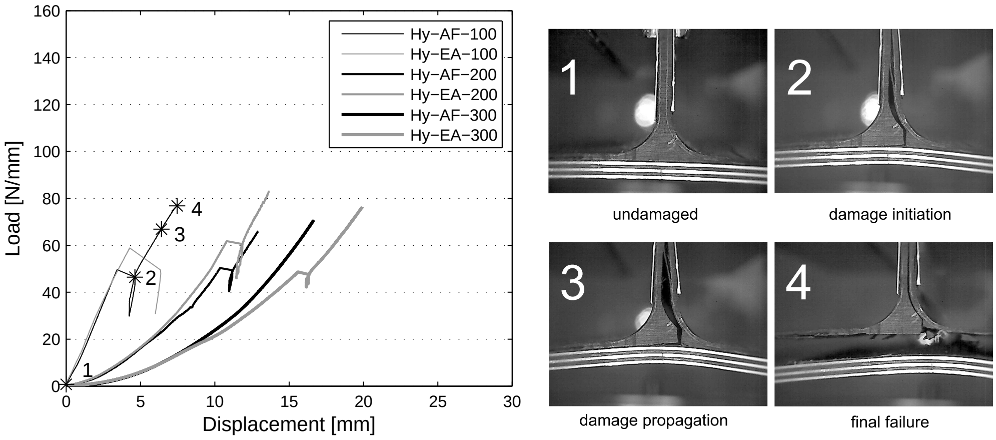

(a) (b)

Figure 3: Typical hybrid joint (a) load-displacement curves for the two adhesives (EA and AF) and three spans (100, 200 and 300 mm) and (b) correspondent failure sequence for AF163 adhesive and 100 mm span (Hy-AF-100).

Table 5 shows the average results of the initiation and maximum load levels for all specimen configurations. For a better comparison, the results are also shown as bar charts with scatter bars in Figure 5.

Comparing the initiation and the maximum loads, the extra load carrying capacity of the hybrid joint after damage initiation can go from 9% up to 64% (Pmax–Hy/Pmax–Hy for AF-300 and EA-200, respectively). The value of this remaining capacity has significantly scatter through out the different test series.

Comparing the maximum loads, metal joints have significantly higher load carrying capacities than hybrid joints (Pmax–Mt/Pmax–Hy). This is more evident for long spans, 200 mm and 300 mm, where the metal joints maximum load is on average 1.8 times higher than the correspondent hybrid joint. For 100 mm, this values is less significant (1.33).

It is also interesting to look at the scatter of the tests results. The scatter is at least double

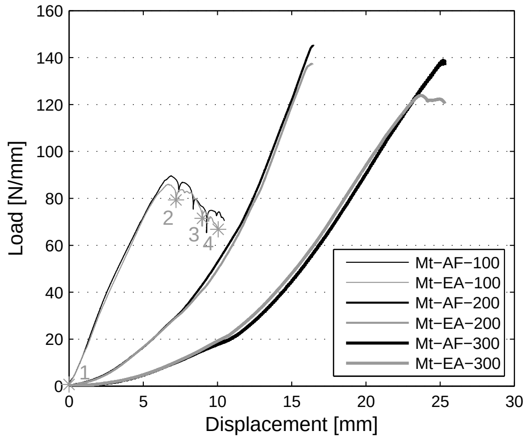

(a) Load-displacement curves

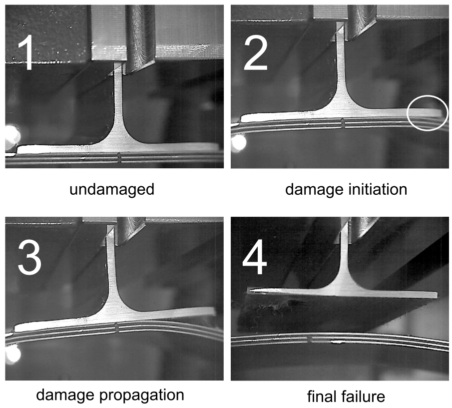

(b) Mt-EA-100 failure sequence

Figure 4: Typical metal joint (a) load-displacement curves for the two adhesives (EA and AF) and three spans (100, 200 and 300 mm) and (b) correspondent failure sequence for EA9696 adhesive and 100 mm span (Mt-EA-100).

for the hybrid joint loads than for the correspondent metal joints. In the hybrid joints the failure occurs in the CFRP stiffener. The stiffener noodles can be potential sites for poor consolidation during manufacturing, which can justify their scattered performance. On the contrary, in the metal joint, where the failure occurred at the adhesive layer, the bond failure was more consistent and robust when compared to the CFRP failure (less scattered).

Concerning the different spans, at the hybrid joints no clear tendency can be observed. For the series using AF 163-2 adhesive, the load carrying capacity increases with the span. However, in the EA 9696 series the maximum load is lower for 300 mm than for 200 mm. The scatter for the hybrid joint series is significant and could be hiding any specific trend, for the span parameter. On the contrary, both adhesive series for metal joints present similar trends; the maximum load increases significantly, about 65%, from 100 mm to 200 mm and decreases about 5% from 200 mm to 300 mm. The results for this series are very consistent which gives more confidence to the trends observed.

Comparing the results of the two adhesives used, for the hybrid joint there is no clear trend once more. In any case, it was not expected that the maximum load would be influenced by the adhesive since the failure occurs at the CFRP stiffener. For metal joints, the series using AF 163-2 have slightly higher maximum load values than the ones using EA 9696 (5%, this value

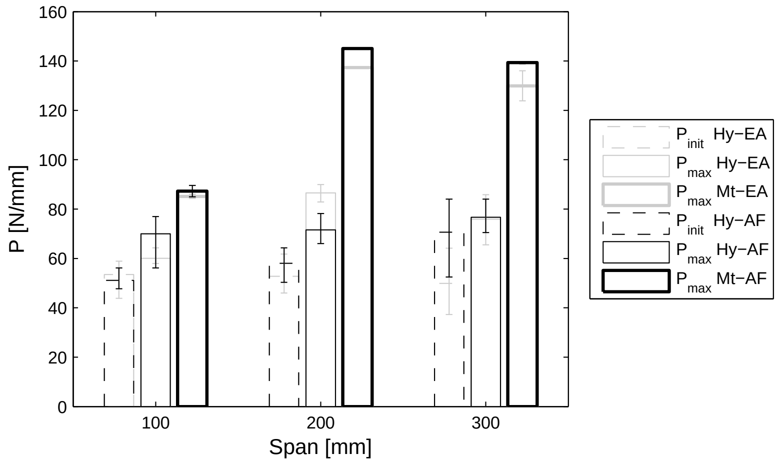

Figure 5: Initiation and maximum loads for hybrid joints (Hy) and metal joints (Mt) and both adhesives EA9696 (EA) and AF 163 (AF), against span.

is lower than the scatter band). The loads are simmilar because the maximum tensile strength of both adhesives is also simmilar (see Table 4).

Table 5: Damage initiation and maximum loads for all pull-off test series (average and coefficient of variation).

	AF-100		AF-200		AF-300		EA-100		EA-200		EA-300	
	Ave (N/mm)	Cv (%)	Ave (N/mm)	Cv (%)	Ave (N/mm)	Cv (%)	Ave (N/mm)	Cv (%)	Ave (N/mm)	Cv (%)	Ave (N/mm)	Cv (%)
Pinit–Hybrid	51.1	9	58.0	10	70.6	19	53.5	13	52.8	15	49.9	22
Pmax–Hybrid	70.0	17	71.6	9	76.7	7	60.0	5	86.6	4	75.9	13
Pmax–Metal	87.3	4	145.1	–	139.3	0.4	85.1	1	137.3	–	129.9	7
Pmax–Hy/Pini–Hy	1.37	–	1.23	–	1.09	–	1.12	–	1.64	–	1.52	–
Pmax–Mt/Pmax–Hy	1.25	–	2.03	–	1.82	–	1.42	–	1.59	–	1.71	–

5. Discussion

In this section, the results of the SPOT will be discussed to evaluate and compare the performance of the metal and the hybrid skin-to-stiffener adhesive joints.

Figure 6(a) compares typical load-displacement curves of the metal joints and of the hybrid joints. Having a metal stiffener or a CFRP stiffener has no influence on the joint stiffness.The joint stiffness are coincident for both joints, at each skin span. Figure 6(b) shows the same curves but the displacement has been normalized with the skin span. It can be observed that the normalized curves of 200 mm and 300 mm span are coincident, while the 100 mm span is significantly different from the formers. This indicates that, although the spans are linearly equidistant between each other (multiples of 100 mm), there is a difference in the bending stiffness of the skin with short-spans (≤ 100 mm span) and long-spans (≥ 200 mm).

In order to reply the question: why is it different, numerical simulations of the SPOT were performed using Finite Element Analysis. The aim is to better understand the joint behaviour and the experimental results.

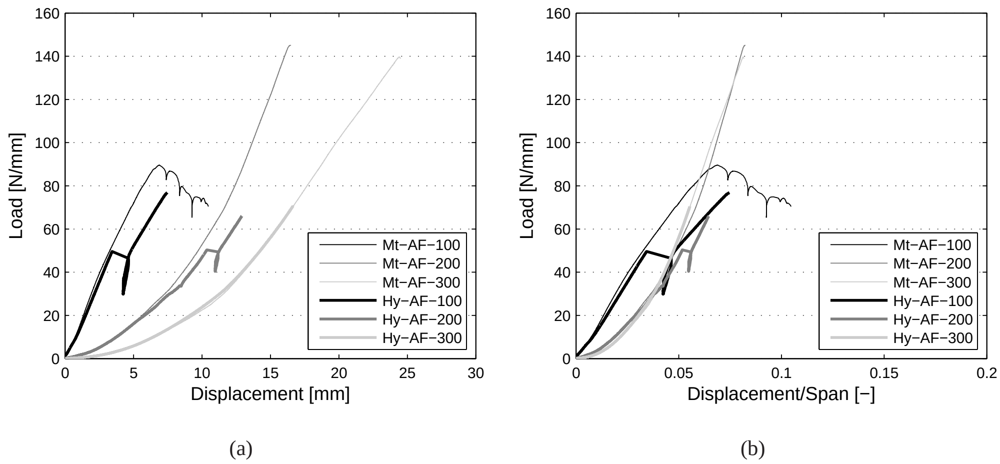

Figure 6: Comparison of the load-displacement curves of the hybrid and metal joints.

5.1. Numerical simulations

Finite Element Analysis were performed to simulate the SPOT. The geometry of the model followed the nominal geometry of the specimens (spans, thicknesses and width). The materials were modeled according to their mechanical properties described in Tables 1 and 2, and for the adhesives Table 4. The loads and boundary conditions were defined to simulate the actual tests; vertical applied load at the stiffeners web and clamping of the skin at the support edges (zero displacements and rotations at the support nodes). The simulations were performed using the commercial FEA program ABAQUS. A three-dimensional model was built using cubic elements. For the parts made of isotropic materials, such as Aluminium stiffener and adhesive layer, C3D20R or C3D20 were used (Continuum 3-Dimensional 20-nodes elements with or without Reduced integration). The reduced integration elements were replaced by full integration elements close to the adhesive bond line, where high peel stress and shear stresses are expected. The parts made

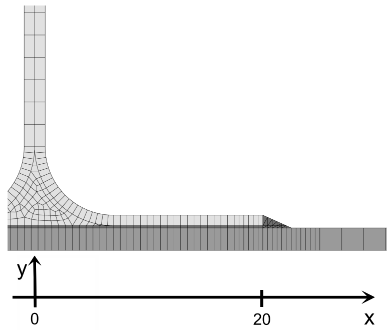

Figure 7: Mesh detail of the Finite Element model (dimensions in mm).

of composites laminates (orthotropic materials) were modeled using C3D20R together with the composite layup feature in ABAQUS. In this feature, the laminate is modeled using one single element per laminate thickness but with 3 integration points per lamina thickness. Different simulations were performed for each span, each stiffener and each adhesive. The mesh size was the same for all models. The FE model had 178574 nodes and 34150 elements. A convergency mesh study was performed to prove the mesh independency of the results. A detail of the mesh is shown in Figure 7.

Load-displacement curves obtained from the experiments are compared with LD curves obtained from the FEM in Figure 8. Consider the hybrid joints curves in Figure 8(a). For short spans (100 mm), the joint behaves linear elastically until the first damage occurs. The simulation using linear elastic material properties and linear geometry predicts very well the bending stiffness of the hybrid joint for 100 mm span. For long spans the scenario is different. The simulations that best predict the joint stiffness for 200 and 300 mm span, has to take into account non-linear geometry effects to simulate the stiffening of the skin. In addition to this, using the elasto-plastic material properties improves slightly the simulation results. However, the stiffness predictions are fairly above the experimental results. This might be due to the fact that, the measured displacement is given by the piston of the machine, which also takes into account all the slips in the specimen and in the test set-up, that shows an extra flexibility to the experimental results. Next consider the metal joint load displacement curves shown in Figure 8(b). The simulations show similar conclusions as for hybrid joints; for short spans elastic and linear geometry FE analysis has the best prediction of the joint stiffness and for long spans non-linear geometry effects must be taken into account for predicting the stiffening of the joint. For 100 mm, the predictions are less good than for hybrid joints. This might be caused to initiation of skin damage at a micro-level before failure that has not been detected in visual observations (delaminations, debonding fibre-matrix, etc.). The results presented are for AF 163-2 adhesive. For EA 9696, the same observations can be found.

In summary, the difference between the short spans and long spans stiffness behaviour found in Figure 6(b) is related with the non-linear geometry effects that play a very significant role for long spans, and can be neglected for short spans.

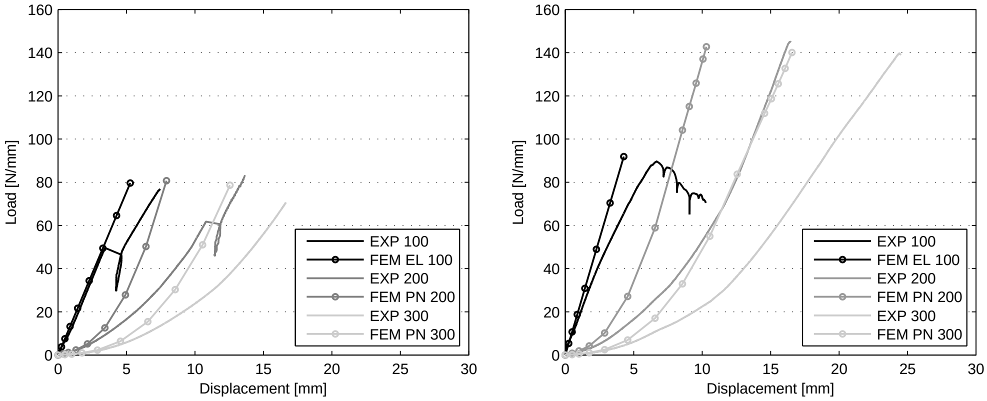

(a) Hybrid joint: AF 163-2

(b) Metal joint: AF 163-2

Figure 8: Comparison between load-displacement curves obtained from the experiments (EXP) and the FEM (EL: Elastic properties/Linear geometry analysis; PN: Elasto-plastic properties/ Non-linear geometry analysis).

5.2. *Fractographic analysis*

Specimens were selected of metal and hybrid joints to conduct a fractography analysis of the failure surfaces. The analysis consisted in, firstly, visually observe the exposed fracture surfaces, secondly, select areas of interest using optical microscopy and finally, fully characterize the fracture surfaces using Scanning Electron Microscope (SEM).

Figure 9 shows the typical fracture surfaces and failure sequence of a Metal joint. The failure mode is mainly cohesive in the adhesive layer. The crack initiated in the adhesive at the tip of the stiffener foot and propagated always through the adhesive, up to the opposite end. This can be confirmed by the remainings of adhesive material on both adherend failure surfaces (see Figure 9(a) stiffener foot and skin). Looking to the SEM fracture surfaces, one can better understand the crack propagation in the adhesive. Figure 10 shows typical surfaces as the crack extended in the AF 163-2 adhesive; from point 1 (start) up to point 5 (end). The rhombus-shape fibers in the fracture surfaces is the adhesive carrier (nylon fibre). The carrier guarantees a minimum adhesive thickness after curing but it has no structural function.

At the crack initiation (point 1), the fracture surface show typical features of mode II loading (shear); shallow cusps can be easily recognizable (photo 1a). The cusps are tilted according to the shear stresses present at that side of the stiffener foot. These features identified in the adhesive resemble resin rich areas of composite laminates under mixed mode I and II [18]. Under pure mode II, the shear cusps are erect and steep [18]. But if mode I is also present, the cusps become more shallow but maintaining the alignment according with the shear stress. This is believed to be also the case in the adhesive fracture from point 1 to point 3; the adhesive is under mixed mode I and II resulting in fracture surfaces with shallow cusps aligned towards the same direction (opposite to the global crack growth).

The fracture surface only changes significantly at approximately 7 to 8 mm from the opposite tip of the stiffener, at point 4. There is no more cusps and the fracture surface is more flat. According to what is reported for resins in composite laminates, some feature of mode I loading can be identified, such as scarps and riverlines [18], indicating that the component of mode I increased and it became dominant at point 4. In the present adhesive the scarps have a concentrical shape with riverlines converging to a center particle. This centre particle is believed to be rubber particles dispersed into the AF 163-2 epoxy to increase its toughness. The riverlines direction indicate that the micro cracks started at the interphase between these dispersed particles and the epoxy resin and grew into the surrounding matrix. Each concentric shape resembles a mushroom seen up side down, where the center particle is the mushroom stem, the scarp is the mushroom cap edge and the riverlines the mushroom gills.

Three to five millimeters from the foot tip, very close to the crack end, the fracture surface presents shallow cusps again, indicating an increase of mode II component (Point 5, photo 5 and 5a). The main difference in the cusps when compared to points 1 to 3 is their tilt direction; in point 1 up to 3 is opposite to the crack growth and in point 5 is towards the crack growth (photo 1a and 5a, respectively). This change is caused by the change in shear stress direction.

The SEM fracture surfaces show that the adhesive is under mixed mode I and II loading. This is according to what was expected since shear stresses and peel stresses are present at the adhesive during pull-off load. The cracks starts under predominantly mode II at the foot tip of the stiffener. The cracks extends toward the opposite foot tip. Mode I component loading increases, and it is dominant at 7 to 8 mm of the crack end. At the very end, immediately before the crack ends, mode II loading increases again.

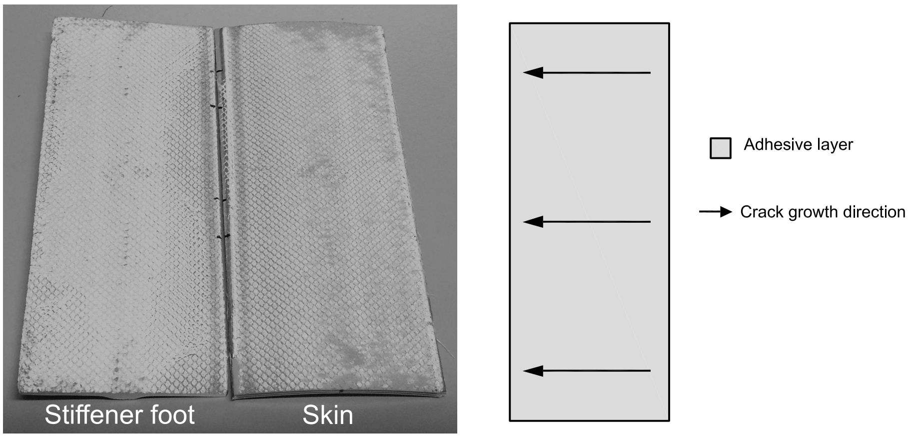

(a) Fracture surfaces (b) Failure sequence: skin surface

Figure 9: Typical fracture surfaces and failure sequence of a Metal joint.

Considering the hybrid joint, Figure 11 shows the typical fracture surfaces and failure sequence. Delamination initiated at the stiffener noodle at the interface between the 0° noodle plies and the 45° L-shape ply (1st stiffener foot ply) – interlaminar failure. Then, the crack extended mainly across the foot 45° ply towards the tip of the foot. In some restricted areas very close to the stiffener noodle, the crack propagated in the adhesive layer (cohesive failure) and in minor areas at the interface stiffener foot/adhesive layer (adhesive failure). Simultaneously, intralaminar failure initiated at the 0° noodle plies towards the tip of the foot and delamination initiated at the interface 45°/90° of the stiffener foot (1st/2nd stiffener foot ply).

Figure 12 show the fracture surfaces observed in SEM. Directly under the stiffener noodle (point 1), mode I is the dominating load for the intralaminar failure of the 0° noodle plies. Typical features at the resin rich areas, such as scarps and riverlines can be easily identified. The delamination between 0° noodle plies and the 45° foot plies in point (2) occurred under mode II loading. The fracture surface presents shallow cusps tilted toward the foot tip. Just adjacent to this (3a), the cusps became flat and replaced by scarps and riverlines, which indicate a mode I dominated failure. At the areas where the cracks grew into the adhesive layer (3b), the fracture

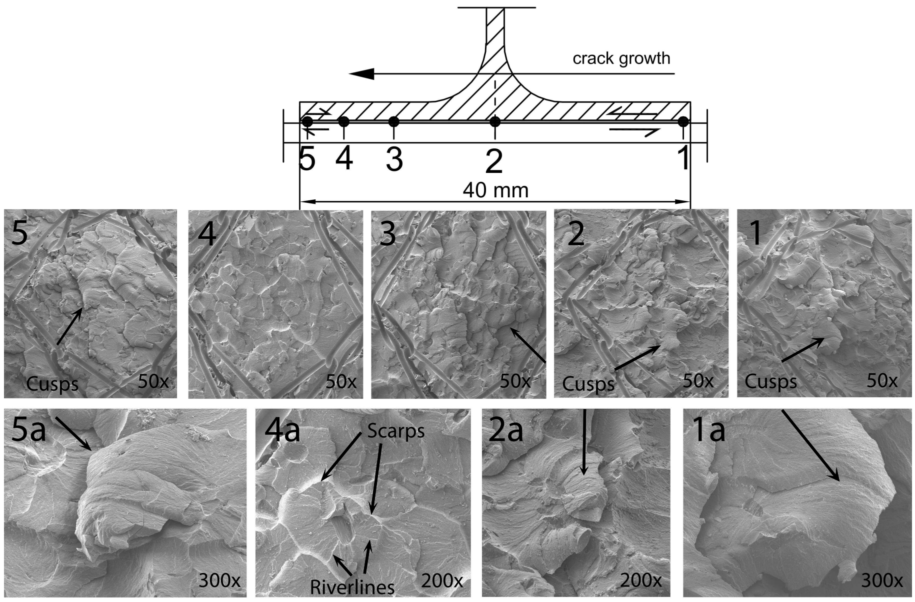

Figure 10: Skin fracture surfaces as the crack extends in the adhesive layer from one tip of the stiffener foot to the opposite tip, in a Metal joint.

in the adhesive is also significantly fat without any cusps. As the crack extended toward the foot tip, mode II loading starts increasing again (point 4), shown by the tilted cusps. At the foot tip (point 5), the failure is clearly dominated by mode II loading. The cusps became steeper and more erected (5a). The tilt direction of the cusps is in accordance with the shear stresses (approximately the crack growth direction). Since the fracture surfaces are quite symmetric, only half of the joint length is shown.

Next it is interesting to compare mode I and mode II features in an adhesive fracture and in a composite laminate fracture. It is expected that the resin rich areas of a composite laminate present similar features as an adhesive, since they are both epoxy resins. However there are still some differences worth to mention. In mode II dominated failure, shear cusps are present in both resin and adhesives, however cusps in composite laminates are much smaller than in adhesives. The shear cusps in composites develop between the carbon fibers and therefore they are smaller than in pure adhesive layers, where they develop between adherends. Furthermore, in the adhesive layer as the shallow cusps have no boundaries, the fracture surfaces resemble a shallow sea at the coast line while in the composite laminates it resembles shallow waves in river

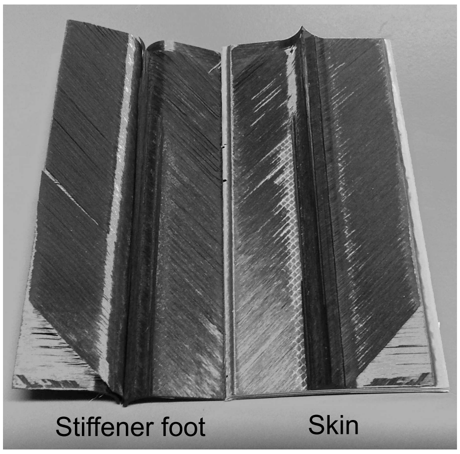

(a) Fracture surfaces

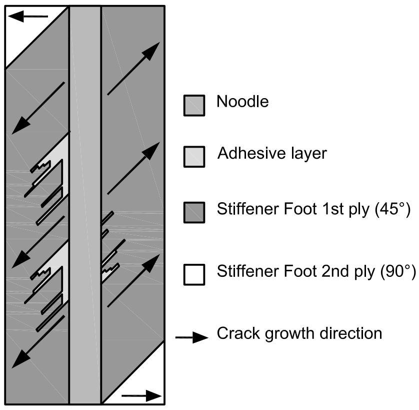

(b) Failure sequence: skin surface

Figure 11: Typical fracture surfaces and failure sequence of a Hybrid joint.

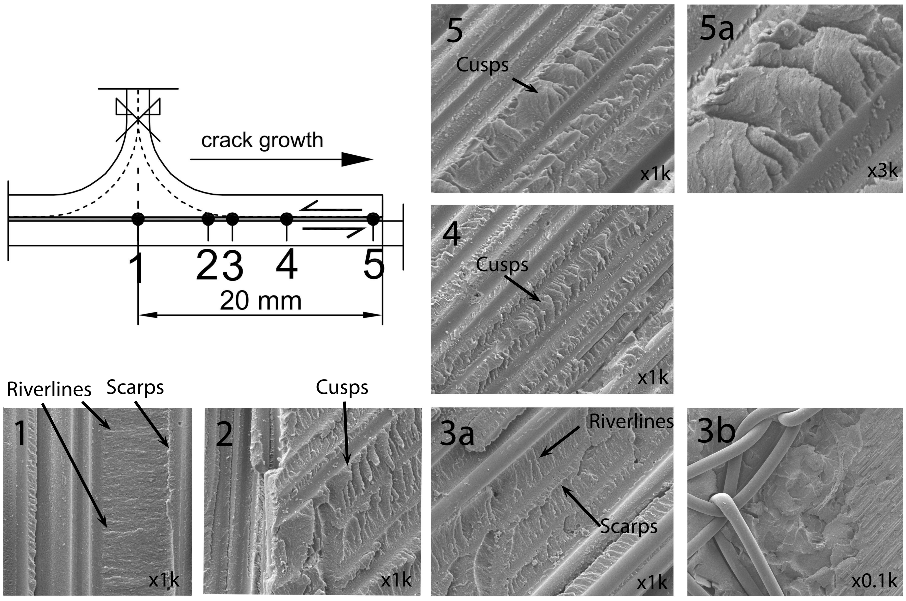

Figure 12: Skin fracture surfaces as the crack extends from the noodle to the end of the stiffener foot, in a Hybrid joint.

channels.

Considering mode I features, on both materials, scarps and riverlines can be identified. Both in composites and in epoxies, the riverlines indicate the micro crack initiation and propagation.

However, for scarps the scenario is different. In composites, scarps tend to be parallel to the fiber and it is claimed to give an indication of the global crack grow. In the adhesive, scarps have more random direction and it certainly do not indicate the global crack growth (concentric shape in photo 4a in Figure 10). Scarps are only the convergence between two adjacent predominant crack planes and do not indicate any regular direction. For the adhesive AF 163-2 studied, as the micro crack started at the dispersed particles, the scarps are at the crack plane of adjacent particles. It is also believed that scarps in composites do not always indicate the global crack growth. This only occurs if the crack growth is aligned with the fibers. The scarps are parallel to the fibers because the micro crack planes are aligned with the fibers and converge in the same direction. If the crack growth is parallel to the fiber, the scarps give a wrong indication of the global crack growth. This is shown in photo 1 in Figure 12, where the global crack direction is from left to right (horizontal), and the scarp direction is vertical (top to bottom).

It is also interesting to relate the failure modes of the two skin-to-stiffener joints with the corresponding maximum loads. The maximum loads associated with intralaminar failure of the composite (hybrid joints) are 40% to 60% lower than the maximum loads associated with cohesive failure of the adhesive (metal joints). This is in accordance with previous results obtained from coupon tests for assessing the adhesion quality of metal bonds and composite bonds. In those tests, the cohesive strength of the adhesive was also higher than the intralaminar strength of the composite laminates. There is a correlation between the results from coupon tests (peel tests) and from subcomponent tests. The results of the coupon tests are extensively reported elsewhere [7].

6. Conclusions

Stiffener Pull-Off Tests were performed on two types of skin-to-stiffener adhesive joints; metal-skin to metal-stiffener (metal joint) and metal-skin to composite-stiffener (hybrid joint). The aim was to compare the failure mechanism and load carrying capacity of both joints, varying the skin span and the type of adhesive. From the analysis of the results and of the fracture surfaces, the following conclusions were drawn:

- In the hybrid joint, the typical initial damage occurs at the noodle region of the composite stiffener. The failure mechanism was interlaminar failure between the 0° noodle plies and the 45° first ply of the stiffener foot, under mode II dominated loading. The initial damage is accompanied by a sudden drop in the load.

- Immediately after the initial delamination, the crack extends mainly through the 45° stiffener foot plies towards the tip of the foot, under mode I dominated intralaminar failure. In restricted areas, the crack extends through the adhesive layer also under mode I predominant loading. Simultaneously, intralaminar failure initiated at 0° noodle plies and interlaminar failure initiated between the 1st and 2nd ply of the stiffener.

- As the crack extended towards the foot tip, mode II component loading increased and at the very end it is clearly the predominant loading type.

- In the metal joints, the damage event occurred entirely in the adhesive layer. The failure mechanism was cohesive failure under mixed mode I/II loading. The crack initiated in the adhesive at the stiffener foot tip, under predominantly mode II. As the crack extended toward the opposite foot tip, mode I component loading increases. At the very end, mode II is again the predominant loading type.

- The flexural stiffness of the skin-to-stiffener joint has two distinct behaviours, depending on the span of the skin. For short-spans (<100 mm), the skin behaves linearly elastic. For long spans (>200 mm and 300 mm), non-linear geometry effects play a significant role and elasto-plastic material behaviour occurs. These two cluster behaviours (short spans and long spans), determine the load carrying capacity of the metal joint; for long spans the maximum load is about 65% higher than for short spans. In the hybrid solutions, there is no influence of the span in the maximum load carring capacity.

- In the metal joint, the maximum load is 1.3 up to 1.8 times higher than for the hybrid solution, for short spans and long spans, respectively. Cohesive failure in the adhesive leads to higher load capacities than inter/intra laminar failure of composites. However, the failure is less damage-tolerant in the adhesive layer than in the composite (no remaining load capacity in the metal solution after initial damage).

- The type of adhesives used in this study has little influence in the behaviour of both skin-to-stiffener solutions.

Acknowledgments

This research was supported by Materials innovation institute (M2i) and Fokker Aerostructures.

[1] Gary Savage. Failure prevention in bonded joints on primary load bearing structures. 14(2):321–348, 2007. *Engineering Fracture Mechanics*, 14(2):321–348, 2007.

[2] J.F.P Owens and P. Lee-Sullivan. Stiffness behaviour due to fracture in adhesively bonded composite-to-aluminum joints II. experimental. *International Journal of Adhesion and Adhesives*, 20(1):47 – 58, 2000.

[3] S. Kang, M. Kim, and C. Kim. Evaluation of cryogenic performance of adhesives using composite-aluminum double-lap joints. *Composite Structures*, 78(3):440 – 446, 2007.

[4] M. Seong, T. Kim, K. Nguyen, J. Kweon, and J. Choi. A parametric study on the failure of bonded single-lap joints of carbon composite and aluminum. *Composite Structures*, 86(13):135 – 145, 2008.

[5] K. Ishii, M. Imanaka, and H. Nakayama. Fatigue crack propagation behavior of adhesively-bonded CFRP/aluminum joints. *Journal of Adhesion Science and Technology*, 21(2):153–167, 2007.

[6] M. Khoshravan and F. A. Mehrabadi. Fracture analysis in adhesive composite material/aluminum joints under mode-I loading; experimental and numerical approaches. *International Journal of Adhesion and Adhesives*, 39(0):8 – 14, 2012.

[7] S. Teixeira de Freitas and J. Sinke. Adhesion properties of bonded composite-to-aluminium joints using peel tests. *The Journal of Adhesion*, 90(5-6):511–525, 2014.

[8] PJ Minguet. Analysis of the strength of the interface between frame and skin in a bonded composite fuselage panel. In *38th AIAA/ASME/ASCE/Ahs/ASC Structures, Structural Dynamics, and Materials Conference and AIAA/ASME/AHS Adaptive Structures Forum: A Collection of Techical Papers*, pages 2783–2790, 1997.

[9] Jian Li, T Kevin O'Brien, and Carl Q Rousseau. Test and Analysis of Composite Hat Stringer Pull‐off Test Specimens. *Journal of the American Helicopter Society*, 42(4):350–357.

[10] J Li. Pull-off tests and analysis of composite skin and frame T-joint. In *17th Annual Technical Conference of the American Society for Composites*, 2002.

[11] Emile Greenhalgh, Aaron Lewis, Richard Bowen, and Marcello Grassi. Evaluation of toughening concepts at structural features in CFRPPart I: Stiffener pull-off. *Composites Part A: Applied Science and Manufacturing*, 37(10):1521–1535, October 2006.

[12] Denis D.R. Cartié, Giuseppe DellAnno, Emilie Poulin, and Ivana K. Partridge. 3D reinforcement of stiffener-to-skin T-joints by Z-pinning and tufting. *Engineering Fracture Mechanics*, 73(16):2532–2540, 2006.

[13] Emile Greenhalgh and Manuel Huertas Garcia. Fracture mechanisms and failure processes at stiffener run-outs in polymer matrix composite stiffened elements. *Composites Part A: Applied Science and Manufacturing*, 35(12):1447–1458, 2004.

[14] Murat Demir Aydin and Salih Akpinar. The strength of the adhesively bonded T-joints with embedded supports. *International Journal of Adhesion and Adhesives*, 50:142–150, 2014.

[15] S. Teixeira de Freitas and J. Sinke. Test method to assess interface adhesion in composite bonding. *Applied Adhesion Science*, 3(1):1–13, 2015.

[16] Rene Alderliesten. *Fatigue crack propagation and delamination growth in Glare*. PhD thesis, Delft University of Technology, 2005.

[17] ISO-527. ISO-527: Plastics - Determination of Tensile Properties, 2012.

[18] Emile Greenhalgh. *Failure analysis and fractography of polymer composites*. Woodhead Publishing Limited, UK, 2009.